Journal of Materials Science & Technology 207 (2025) 105–112

Contents lists available at ScienceDirect

Journal of Materials Science & Technology

journal homepage: www.elsevier.com/locate/jmst

Research Article

Obtaining extremely low coercivity of high B_s FeCoBSiCPCu nanocrystalline alloys through modulation of magnetic anisotropy

Mingjuan Cai, Zhijun Guo*, Lei Li, Xingyu Zheng, Xiaoxuan Yang, Qianqian Liu, Gaopeng Zou, Baolong Shen*

School of Materials Science and Engineering, Jiangsu Key Laboratory for Advanced Metallic Materials, Southeast University, Nanjing 211189, PR China

ARTICLE INFO

Article history:
Received 29 January 2024
Revised 1 April 2024
Accepted 3 April 2024
Available online 11 May 2024

Keywords:
Nanocrystalline alloy
Magnetic anisotropy
Magnetic field annealing
Soft-magnetic property
Microstructure

ABSTRACT

Longitudinal magnetic field annealing is utilized for modifying the magnetic anisotropy and enhancing the magnetic softness of $Fe_{75}Co_8(B_{10}Si_3C_3P_1)_{1-x/17}Cu_x$ (x = 0.5, 0.75, 1, 1.25) nanocrystalline alloys. All of the magnetic field-annealed nanocrystalline alloys with Cu content more than 0.5 at.% exhibit significantly improved soft-magnetic properties, including high saturation magnetic flux density up to 1.87 T, effective permeability of 13,000–16,000 under the condition of 1 A/m and 1 kHz, coercivity as low as 1.6 A/m, and core loss of 0.11–0.45 W/kg under the condition of 1.0 T and 50 Hz. The application of a magnetic field promotes the nucleation and inhibits the growth of grains, leading to an increase in the number density of nanocrystals and the crystalline volume fraction, and a reduction in the grain size. The magnetic field annealing reduces the effective magneto-crystalline anisotropy energy to 2–4 J/m^3, and induces longitudinal magnetic anisotropy with anisotropy energy density of 400–900 J/m^3 which shows dependence on the crystalline volume fraction. The field-induced magnetic anisotropy dominates over the random local magnetic anisotropies, and results in the formation of regular magnetic domains aligned longitudinally, pinning-free domain wall displacement, and thus enhanced soft-magnetic properties.

1. Introduction

Fe-based nanocrystalline soft-magnetic alloys have attracted considerable attention due to their low core loss and high energy conversion efficiency [1]. Compared with silicon steels, the considerably reduced effective magneto-crystalline anisotropy energy gives intrinsically small hysteresis loss, and an order of magnitude reduction in thickness and about twice higher electrical resistivity contribute to lower eddy current loss [2,3]. However, their relatively low saturation magnetic flux density (B_s) has become the main limitation to the applications in high-power-density scenarios [4]. Great efforts have been devoted to improving the B_s of Fe-based nanocrystalline alloys by increasing the content of ferromagnetic elements [5,6]. Nevertheless, these Fe-metalloid and Fe-metalloid-Cu nanocrystalline alloys suffer from poor amorphous-forming ability, harsh nucleation-growth processes, and deterioration of soft-magnetic properties [7,8]. How to balance the relationship among the B_s, amorphous-forming ability and soft-magnetic property is a major challenge.

Recently, through partial substitution of Fe by Co, the $Fe_{75}Co_8B_{10}Si_3C_3P_1$ amorphous alloy was developed with relatively high B_s, wide crystallization temperature interval, and good amorphous-forming ability, which promises the flexibility in manufacturing [9]. It has been widely reported that the Cu element segregates to Cu or CuP clusters prior to the onset of primary crystallization due to the positive mixing enthalpy (ΔH, +13 kJ/mol) between Fe and Cu and negative ΔH (−9 kJ/mol) between P and Cu, which promotes the heterogeneous nucleation and refines the grain [10]. Therefore, based on the $Fe_{75}Co_8B_{10}Si_3C_3P_1$ alloy, the $Fe_{75}Co_8(B_{10}Si_3C_3P_1)_{1-x/17}Cu_x$ (x = 0.5, 0.75, 1, 1.25) nanocrystalline alloys were fabricated to construct the nanoscale nanocrystalline-amorphous microstructures and were denoted as the Cu0.5, Cu0.75, Cu1 and Cu1.25 alloys, respectively. However, Co substitution tends to increase the magnetic anisotropy due to the large magneto-crystalline anisotropy constant K_1 of Co element [11] and large incoherent induced magnetic anisotropies originating from the pair ordering of Co atoms in the nanocrystals, resulting in the deteriorated magnetic softness [12]. The modulation of

* Corresponding authors.
E-mail addresses: zj-guo@seu.edu.cn (Z. Guo), blshen@seu.edu.cn (B. Shen).

https://doi.org/10.1016/j.jmst.2024.04.047
1005-0302/

magnetic anisotropy by magnetic field annealing or stress annealing plays an important role in controlling the shape of hysteresis curve according to the application requirements [9,12]. It has been documented that longitudinal magnetic field annealing (FA) induces long-range magnetic anisotropy with an easy axis parallel to the applied field and more effectively achieves superior soft-magnetic properties including high permeability and low coercivity (H_c) compared with stress annealing in Finemet, Nanoperm, and Hitperm nanocrystalline alloys [13,14].

Therefore, in this work, the effectiveness of the FA process on the soft-magnetic properties, microstructure, magnetic anisotropy, and magnetization process was systematically investigated for the Cu0.5, Cu0.75, Cu1 and Cu1.25 nanocrystalline alloys. The FA-treated nanocrystalline alloys with Cu content more than 0.5 at.% show high B_s of 1.84–1.87 T, high effective permeability (μ_e) up to 16,000 under the condition of 1 A/m and 1 kHz, low H_c of 1.6–3.0 A/m, and core loss (P_{cm}) as low as 0.11 W/kg under the condition of 1.0 T and 50 Hz. The significant enhancement of soft-magnetic properties is mainly attributed to the longitudinal field-induced anisotropy K_u (400–900 J/m^3) dependent on crystalline volume fraction (V_c), which dominates over the local magnetization-induced anisotropies and suppresses the anisotropy fluctuations, as well as the small average magneto-crystalline anisotropy $\langle K_1 \rangle$ (2–4 J/m^3) related to the magnetic-field-assisted fine and uniform dual-phase nanostructure. This work provides novel insights into the modulation of nanostructure and magnetic anisotropy distribution of high B_s Fe-based nanocrystalline alloys.

2. Material and methods

The alloy ingots with nominal atomic compositions of $Fe_{75}Co_8(B_{10}Si_3C_3P_1)_{1-x/17}Cu_x$ (x = 0.5, 0.75, 1, 1.25) were prepared by induction melting the mixtures of pure elements of Fe (99.99 wt.%), Co (99.99 wt.%), B (99.99 wt.%), Si (99.999 wt.%), Cu (99.99 wt.%), and pre-alloys of Fe-P (26.4 wt.% P) and Fe-C (5 wt.% C) in highly purified argon atmosphere. The as-quenched (AQ) ribbons with an approximate thickness of 20 μm and width of 1 mm were fabricated by a single roller melt spinning technique. The ribbons with a length of 50 mm were subjected to a longitudinal FA process isothermally for 2 min under high vacuum condition and a subsequent water quenching, with a magnetic field strength of 0.1 T. For comparison, the normal annealing (NA) process was carried out without a magnetic field. The AQ and FA/NA-treated $Fe_{75}Co_8(B_{10}Si_3C_3P_1)_{1-x/17}Cu_x$ (x = 0.5, 0.75, 1, 1.25) ribbons were labeled as Cux-AQ and Cux-FA/NA-annealing temperature, respectively. The microstructure was characterized by the X-ray diffraction (XRD, Bruker D8-Discover) with Cu K_α radiation, and the high-resolution transmission electron microscopy (HRTEM, Talos F200X) equipped with energy-dispersive X-ray spectroscopy (EDS). The average grain size (D_{av}) of nanocrystals was estimated by fitting the grain size distribution of nanocrystals in the selected bright-field TEM image. The number density (N_d) of nanocrystals was estimated by using $N_d = N / (A \times D_{av})$, where N represents the quantity of nanocrystals and A represents the area of the TEM image. The V_c of nanocrystals was estimated by $V_c = N_d \pi {D_{av}}^3/6$ [15]. The thermal properties were analyzed using the differential scanning calorimeter (DSC, Netzsch 404 F3). The initial magnetization curves and hysteresis loops were measured by the vibrating sample magnetometer (VSM, Lake Shore 7407), and the B_s was determined under an applied field of 800 kA/m. The H_c, μ_e at 1 kHz, and P_{cm} were measured by a DC B-H loop tracer (Riken BHS-40) under a maximum applied field of 1 kA/m, an impedance analyzer (Keysight, E4990A) under a field of 1 A/m, and an AC B-H loop tracer (Riken AC BH-100 K), respectively. The magnetic domain patterns were observed employing a magneto-optical Kerr microscope (Evico Magnetics GmbH, em-Kerr-highres).

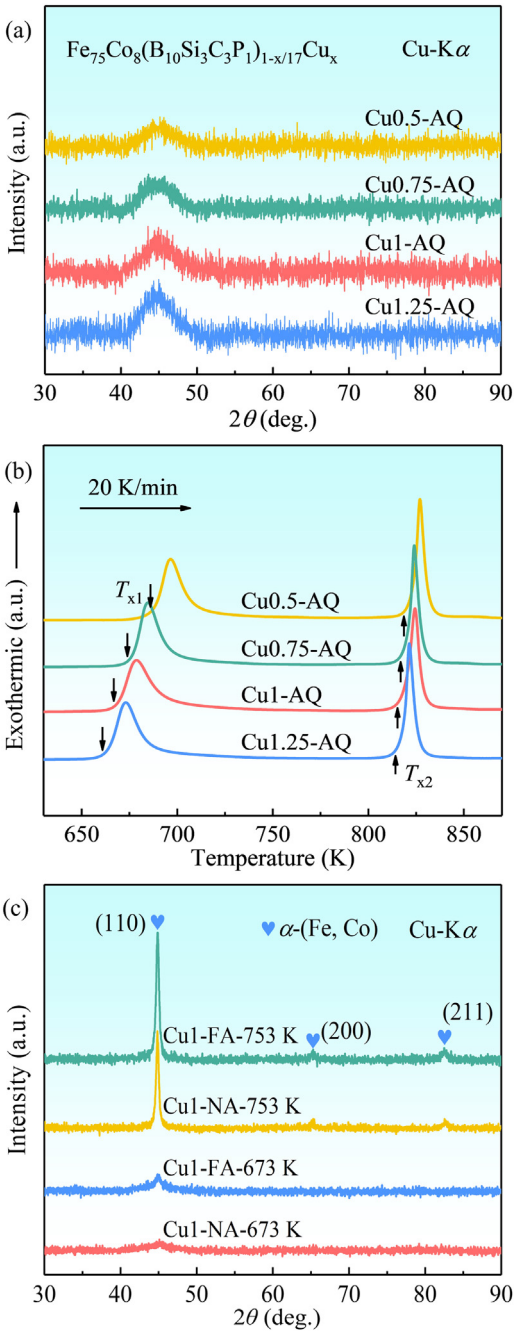

Fig. 1. (a) XRD patterns and (b) DSC curves of Cu0.5-AQ, Cu0.75-AQ, Cu1-AQ, and Cu1.25-AQ samples; (c) XRD patterns of Cu1-FA-753 K, Cu1-NA-753 K, Cu1-FA-673 K and Cu1-NA-673 K samples.

3. Results and discussion

All the AQ ribbon samples with different Cu contents show the amorphous structure as revealed by the XRD patterns of Fig. 1(a). Only broad humps without any distinct crystallization peak can be observed, which suggests that minor Cu addition cannot deteriorate the amorphous-forming ability of these alloys. The DSC curves of AQ samples are displayed in Fig. 1(b), which exhibit a two-stage crystallization process corresponding to the precipitation of α-(Fe, Co) and Fe-metalloid compounds. With the increase of Cu content, the primary crystallization temperature (T_{x1}) gradually decreases from 684 K to 662 K, and the secondary crystallization temperature (T_{x2}) slightly decreases from 818 K to 814 K, increasing the

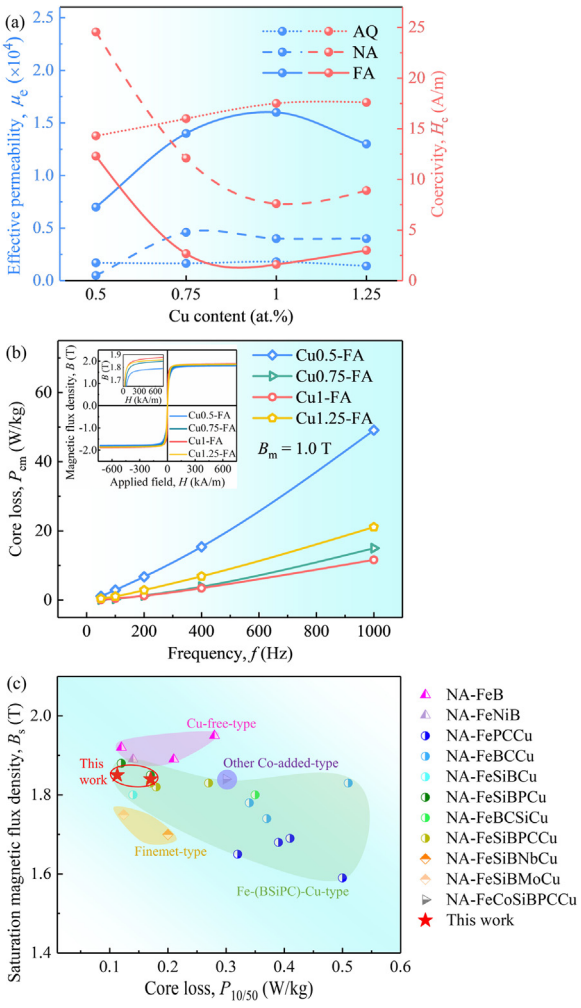

Fig. 2. (a) Changes in μ_e and H_c as a function of Cu content for samples at AQ state and subjected to FA and NA treatments at optimal conditions; (b) Frequency dependence of P_{cm} measured at 1.0 T and hysteresis loops (inset) of Cu0.5-FA, Cu0.75-FA, Cu1-FA and Cu1.25-FA samples treated at optimal conditions; (c) A summary of B_s and $P_{10/50}$ of the nanocrystalline alloys prepared in this work and other typical Fe-based nanocrystalline alloys.

crystallization temperature interval ($\Delta T_x = T_{x2} - T_{x1}$) from 134 K to 152 K. According to the DSC results, FA and NA processes were conducted at different temperatures in the range of 670–770 K. The XRD patterns of Cu1-FA and Cu1-NA samples are shown in Fig. 1(c) as representatives. When the annealing is conducted at 753 K, both samples exhibit obvious crystallization peaks relating to the (110), (200) and (211) reflections of the crystalline α-(Fe, Co) phase, respectively. It is worth noting that the FA sample has a higher intensity of the (110) peak compared with the NA sample, revealing a higher V_c [15]. When the annealing is conducted near T_{x1} (673 K), the FA sample exhibits a noticeable crystallization peak corresponding to the (110) plane of α-(Fe, Co) phase while the NA sample maintains the amorphous structure. Similar results have been found in $Fe_{73.5}Si_{13.5}B_9Nb_3Cu_1$ and $Fe_{78}Si_9B_{13}$ alloys, which reveal that the magnetic field causes the preferential nucleation of (110)-oriented crystals [16,17].

The FA and NA treatments have different impacts on the soft-magnetic properties of ribbon samples with different Cu contents. Fig. 2(a) shows the μ_e and H_c of Cu0.5, Cu0.75, Cu1 and Cu1.25 nanocrystalline alloys subjected to NA or FA treatments at optimum conditions, as well as the AQ samples. Compared with AQ samples, the Cu0.5-NA sample exhibits unimproved μ_e and higher H_c, whereas the Cu0.75-NA, Cu1-NA and Cu1.25-NA samples show higher μ_e and lower H_c. For all the alloys especially those with Cu content more than 0.5 at.%, the FA treatment is much more effective in increasing μ_e and decreasing H_c than the NA treatment. It is noticeable that the values of μ_e increase from 7000 for the Cu0.5-FA sample to 13,000–16,000 for the Cu0.75-FA, Cu1-FA and Cu1.25-FA samples, and corresponding values of H_c decrease from 12.3 A/m to 1.6–3.0 A/m. Fig. 2(b) displays the P_{cm} at 1.0 T with respect to the frequency of Cu0.5, Cu0.75, Cu1 and Cu1.25 nanocrystalline alloys subjected to optimal FA treatments. The P_{cm} of all the samples increases with increasing frequency and decreases significantly when the Cu content is more than 0.5 at.%. The core loss under the condition of 1.0 T and 50 Hz ($P_{10/50}$) decreases from the value of 1.11 W/kg for the Cu0.5-FA sample to the values of 0.11–0.45 W/kg for the Cu0.75-FA, Cu1-FA and Cu1.25-FA samples. The hysteresis loops of Cu0.5, Cu0.75, Cu1 and Cu1.25 nanocrystalline alloys subjected to optimal FA treatments are shown in the inset. The B_s of the nanocrystalline alloys increases gradually from 1.79 T to 1.87 T with increasing Cu content from 0.5 at.% to 1 at.%, and decreases very slightly when the Cu content reaches 1.25 at.%. It has been proved that the B_s relates to the V_c and can be expressed as $B_s = B_{sc}V_c + B_{sa}V_a$, where B_{sa} (B_{sc}) and V_a denote the saturation magnetic flux density and volume fraction of the amorphous (crystalline) phase, respectively. As the B_{sc} is larger than the B_{sa}, the increase of B_s with increasing Cu content may be attributed to an increase in the volume fraction of α-(Fe, Co) phase [18]. Above soft-magnetic properties are summarized in Table 1. The B_s and $P_{10/50}$ of Cu0.75-FA and Cu1-FA samples are compared with other typical Fe-based nanocrystalline alloys [19-32], as shown in Fig. 2(c). The nanocrystalline alloys prepared by the FA method in this work exhibit an excellent combination of high B_s up to 1.87 T and low $P_{10/50}$ as low as 0.11 W/kg, which facilitates their practical applications in electrical industries.

To reveal the structural origin of drastic differences in soft-magnetic properties between FA and NA samples, the microstructure of Cu1 alloy annealed at optimal conditions is investigated as a representative due to its best soft-magnetic properties. As shown in Fig. 3(a, d), a homogeneously distributed nanocrystalline structure composed of fine spherical α-(Fe, Co) grains with D_{av} of 13 nm is formed for the Cu1-FA-753 K sample, while the Cu1-NA-753 K sample has a coarse square-shaped grain structure with D_{av} of 21 nm. The insets in the lower right corners reveal that the Cu1-FA-753 K sample has a grain size distribution ranging from 7 nm to 21 nm, which is much narrower than the Cu1-NA-753 K sample with the distribution ranging from 7 nm to 47 nm. The V_c is evaluated to be 67 % and 50 % for the Cu1-FA-753 K and Cu1-NA-753 K samples, respectively, and the corresponding N_d is evaluated to be 5.6×10^{23} and 1.1×10^{23} m^{-3}. The $\langle K_1 \rangle$ can be calculated by the following equation [33]:

$$\langle K_1 \rangle = |K_1| \cdot V_c^2 \cdot (D/L_0)^6 \quad (1)$$

where D and L_0 denote the grain size and characteristic minimum scale below which the direction of magnetization cannot vary appreciably, respectively. The K_1 is 8200 J/m^3 for bcc $Fe_{80}Si_{20}$ [34] and L_0 is approximately 40 nm for Fe-based alloys [35]. The values of $\langle K_1 \rangle$ are determined to be 4 and 43 J/m^3 for the Cu1-FA-753 K and Cu1-NA-753 K samples, respectively, which indicates that the $\langle K_1 \rangle$ is more efficiently averaged out for the former, rendering its excellent soft-magnetic properties. Fig. 3(b, e) shows the HAADF-STEM images and corresponding EDS mappings. For both Cu1-FA-753 K and Cu1-NA-753 K samples, the Fe and Co atoms exhibit a similar distribution and form enriched areas related to the location of nanocrystals, and the Si, C and Cu atoms are uniformly distributed. It is noted that the P atoms are excluded from nanocrystals and enriched in the residual amorphous matrix for the Cu1-NA-753 K sample as shown in Fig. 3(e-3), whereas ex-

Table 1
Soft-magnetic properties, structural parameters and anisotropy energy density of $Fe_{75}Co_8(B_{10}Si_3C_3P_1)_{1-x/17}Cu_x$ (x = 0.5, 0.75, 1, 1.25) nanocrystalline alloys subjected to optimal NA or FA treatments.

Alloys	Soft-magnetic properties							Structural parameters						Anisotropy energy density		
	μ_e ($\times 10^4$)		H_c (A/m)		$P_{10/50}$ (W/kg)		B_s (T)	D_{av} (nm)		V_c (%)		N_d ($\times 10^{23}$ m^{-3})		$<K_1>$ (J/m^3)		K_u (J/m^3)
	FA	NA	FA	NA	FA	NA	FA	FA	NA	FA	NA	FA	NA	FA	NA	FA
x = 0.5	0.7	0.1	12.3	24.6	1.1	1.4	1.79	–	–	–	–	–	–	–	–	–
x = 0.75	1.4	0.5	2.7	12.1	0.17	0.52	1.84	14	–	49	–	3.4	–	4	–	404
x = 1	1.6	0.4	1.6	7.6	0.11	0.37	1.87	13	21	67	50	5.6	1.1	4	43	867
x = 1.25	1.3	0.4	3.0	8.9	0.45	0.60	1.86	12	–	60	–	6.6	–	2	–	517

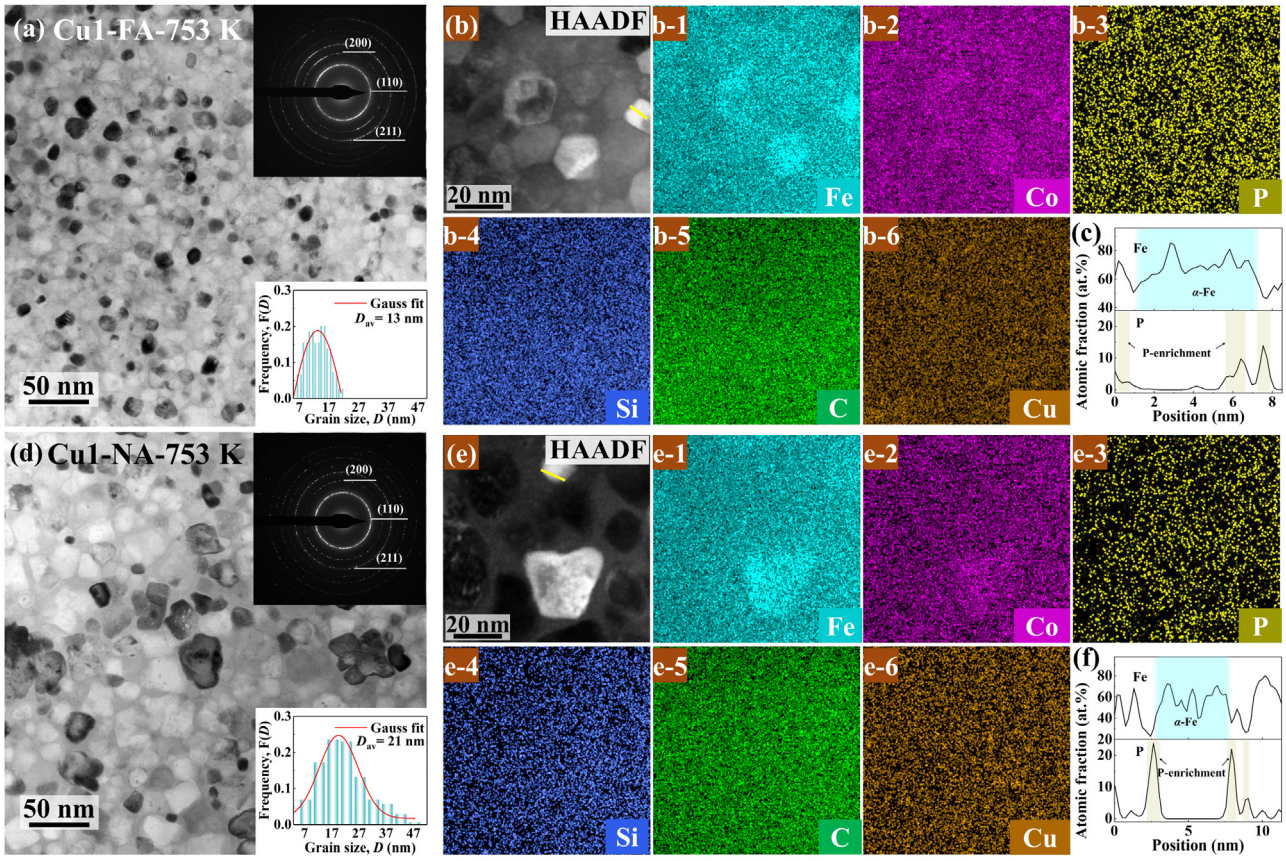

Fig. 3. (a, d) Bright-field TEM images, SAED patterns and grain size distributions; (b, e) HAADF-STEM images and mappings of element distribution of (b) Cu1-FA-753 K and (e) Cu1-NA-753 K samples. Line scans showing the distribution of Fe and P elements across the regions indicated by the yellow lines for (c) Cu1-FA-753 K and (f) Cu1-NA-753 K samples.

hibit a less significant segregation for the Cu1-FA-753 K sample as shown in Fig. 3(b-3). In addition, the atomic line scan measurements (Fig. 3(c, f)) more clearly show the enrichment of P atoms around the α-Fe grain boundary, and indicate that the external field applied during annealing retards the diffusion of P atoms and promotes them a more homogeneous distribution. The magnetic field effect on the P diffusion by the interstitial mechanism may result from an increase in the activation barrier for diffusion jumps due to the magnetic field-induced magnetic ordering [36,37] and thus suppresses grain growth.

To further explore the effect of magnetic field on nanocrystallization, TEM characterizations are also conducted for the Cu1-FA-670 K and Cu1-NA-670 K samples. Fig. 4(a, e) shows the HRTEM images and selected area electron diffraction (SAED) patterns, which reveal no crystallization behavior. The regions highlighted by white squares are divided into cells with a size of 1.707 nm × 1.707 nm and then transformed into 2D auto-correlation maps (Fig. 4(b, f)) to estimate the local transitional symmetry. It is found that the FA treatment promotes local ordering, and the fraction of crystal-like ordering structures for the Cu1-FA-670 K and Cu1-NA-670 K samples is 23 % and 14 %, respectively. In the HAADF-STEM images presented in Fig. 4(c, g), the Cu1-FA-670 K sample exhibits a more obvious bright-dark contrast and apparent larger bright regions with sizes of 2–5 nm than the Cu1-NA-670 K sample. The visible chemical fluctuation related to the heterogeneous contrast cannot be detected in the EDS mappings, which show a relatively homogeneous distribution of Fe, Co, Cu and P atoms for both the Cu1-FA-670 K and Cu1-NA-670 K samples. However, according to the line scan as shown in Fig. 4(d), it is noted that these large bright regions in the Cu1-FA-670 K sample correspond to α-Fe grains and the Cu atoms tend to segregate into clusters with a size of approximately 2 nm, which are located at

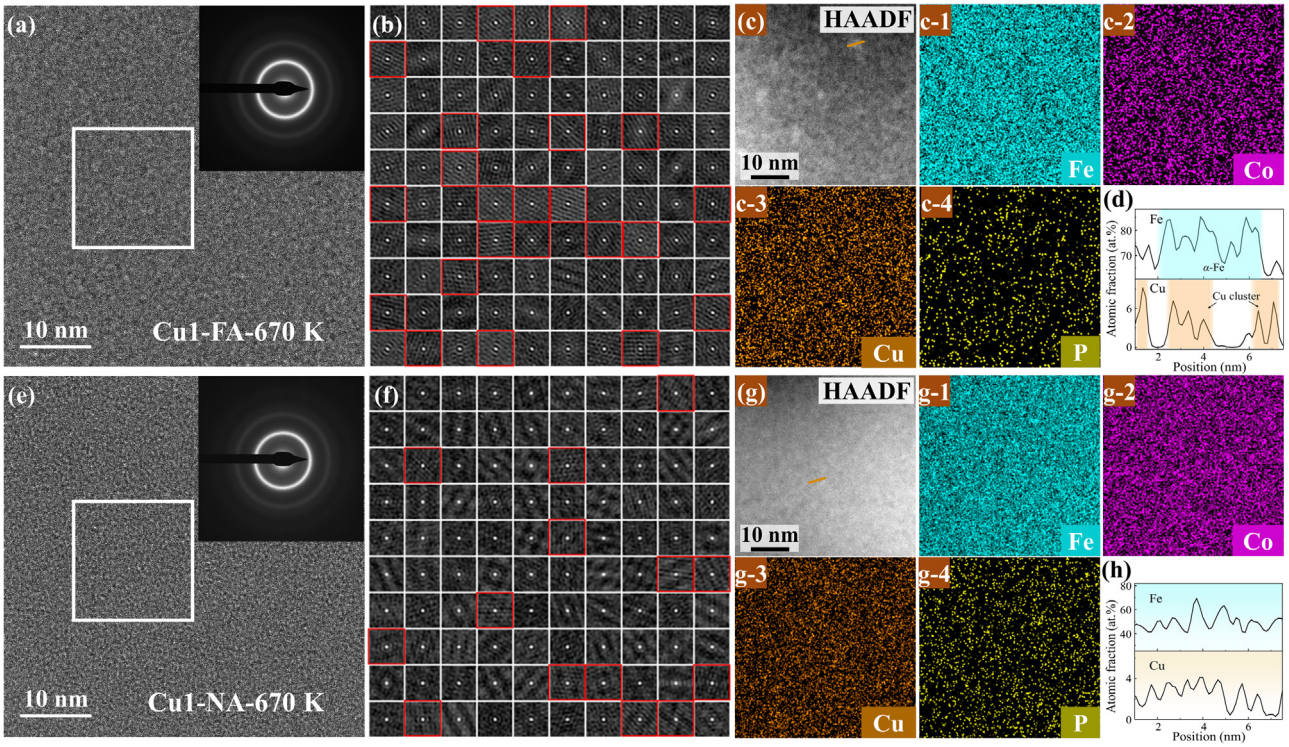

Fig. 4. (a, e) HRTEM images, SAED patterns; (b, f) 2D autocorrelation function analysis of the white squares in (a, e); (c, g) HAADF-STEM images and mappings of element distribution of (c) Cu1-FA-670 K and (g) Cu1-NA-670 K samples. Line scans showing the distribution of Fe and Cu elements across the regions indicated by the orange lines for (d) Cu1-FA-670 K and (h) Cu1-NA-670 K samples.

the grain boundaries and inside the grains. In comparison, the Fe and Cu elements of the Cu1-NA-670 K sample are relatively uniformly distributed as shown in Fig. 4(h).

Based on the above XRD and TEM analyses, it can be concluded that a magnetic field promotes nucleation and inhibits the growth of the grains. In addition to the magnetic contribution to volume-free energy [38], the preferential formation of (110)-oriented nuclei facilitated by the magnetic field decreases the interfacial energy through a suitable match with the (111) plane of Cu clusters [39] and decreases the magneto-crystalline anisotropy energy through orientating with easy axes concentrated near the direction of the magnetic field applied during annealing [16,40]. These magnetic field effects lower the nucleation activation energy and increase the nucleation rate. Besides, the grain growth in the Cu1-FA-753 K sample is suppressed by the competition for growth among a larger number of nuclei [41] and the lower diffusion rate of P atoms by interstitial mechanism compared to those in the Cu1-NA-753 K sample, leading to the reduction of growth rate and thus a finer nanostructure.

In addition to the magnetic field contribution, the optimization of soft-magnetic properties by Cu content adjustment cannot be ignored. The origin of the differences in soft-magnetic properties among these FA-treated nanocrystalline alloys with different Cu contents is discussed in terms of the microstructure and magnetic anisotropy. Fig. 5(a–c) shows the bright-field TEM images of the Cu0.75-FA-753 K, Cu1-FA-753 K, and Cu1.25-FA-753 K samples annealed at optimal conditions. All the samples exhibit dense and ultrafine nanocrystals uniformly embedded in the residual amorphous phase. The insets reveal a similar grain size distribution ranging from 7 nm to 23 nm, with D_{av} of 14, 13 and 12 nm, respectively. The V_c is evaluated to be 49 %, 67 % and 60 %, respectively, and the corresponding N_d is evaluated to be 3.4×10^{23}, 5.6×10^{23} and 6.6×10^{23} m^{-3}. Therefore, the values of $\langle K_1 \rangle$ are determined to be 4, 4 and 2 J/m^3, respectively.

To estimate the values of K_u, the initial magnetization curves were measured transversal to the ribbon axis of the Cu0.75-FA/NA-753 K, Cu1-FA/NA-753 K and Cu1.25-FA/NA-753 K samples and corrected for the demagnetization effect. As shown in Fig. 6(a–c), compared with the NA samples, all the FA samples exhibit an evident linear behavior, which is the characteristic of magnetization process governed by coherent moment rotation and reveals the induction of uniaxial magnetic anisotropy with longitudinal easy axis. The deviation from linearity in the approach-to-saturation region reflects inhomogeneous rotational processes possibly resulting from the effect of dipolar stray fields around α-Fe nanocrystals [42] and is excluded from the determination of K_u. By extrapolating the initial slop, the K_u is calculated as the area between the magnetization curves of FA and NA samples. The values of K_u are 404, 867 and 517 J/m^3 for the Cu0.75-FA-753 K, Cu1-FA-753 K and Cu1.25-FA-753 K samples, respectively, roughly proportional to the corresponding anisotropy field H_k of 497, 1070 and 647 A/m. These typical structural parameters and magnetic anisotropy energy density can also be seen in Table 1.

A detailed analysis of the nanostructure-magnetic anisotropy-magnetic property relationship is carried out here. Fig. 7(a) displays the variation trend of D_{av}, V_c and $\langle K_1 \rangle$ with the Cu content, which verifies the correlation between the changes in B_s (inset of Fig. 2(b)) and V_c, and demonstrates that the slight change of $\langle K_1 \rangle$ related to ultrafine nanocrystals is not responsible for the distinct difference in soft-magnetic properties among the Cu0.75-FA-753 K, Cu1-FA-753 K and Cu1.25-FA-753 K samples. Fig. 7(b) exhibits the variation trend of V_c, K_u and $K_u/\langle K_1 \rangle$ with the Cu content, suggesting the dependence of K_u on the V_c. It has been documented that the K_u of nanocrystalline alloys is mainly attributed to the local K_u contributions from the α-Fe nanocrystals, which may originate from the atomic pair ordering of substitutional Si/Co atoms and directional ordering of interstitial B atoms induced by changing the crystal symmetry [12]. Therefore, the K_u is sensitive to the compo-

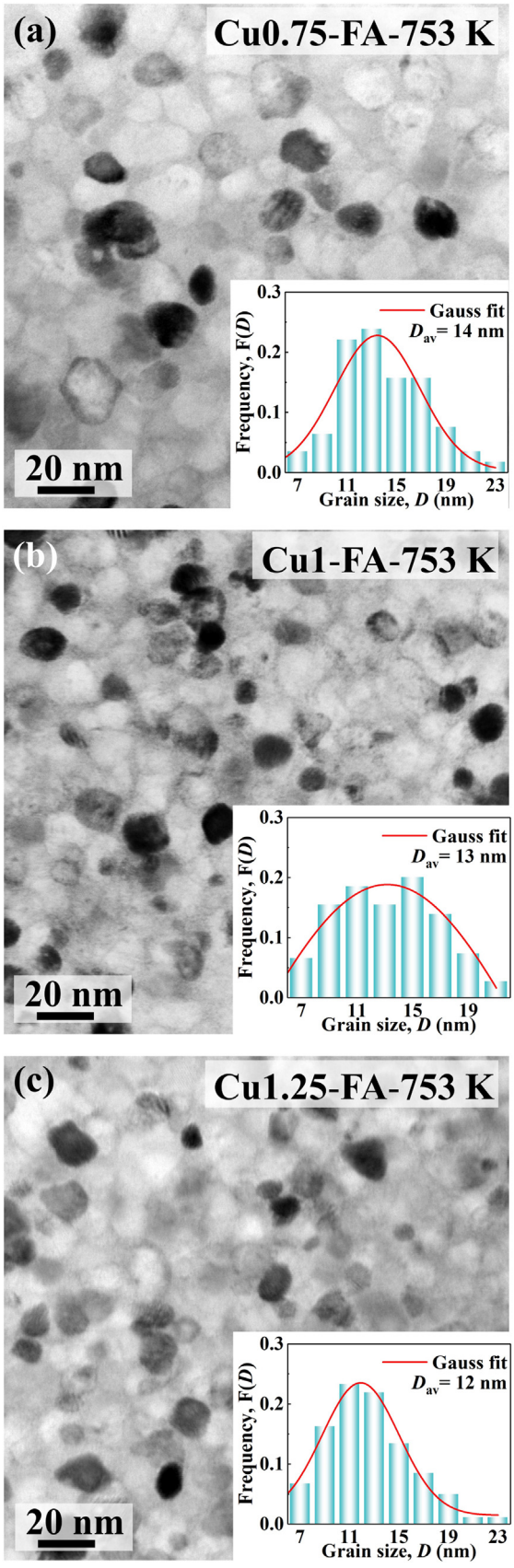

Fig. 5. Bright-field TEM images and grain size distributions of (a) Cu0.75-FA-753 K, (b) Cu1-FA-753 K, (c) Cu1.25-FA-753 K samples.

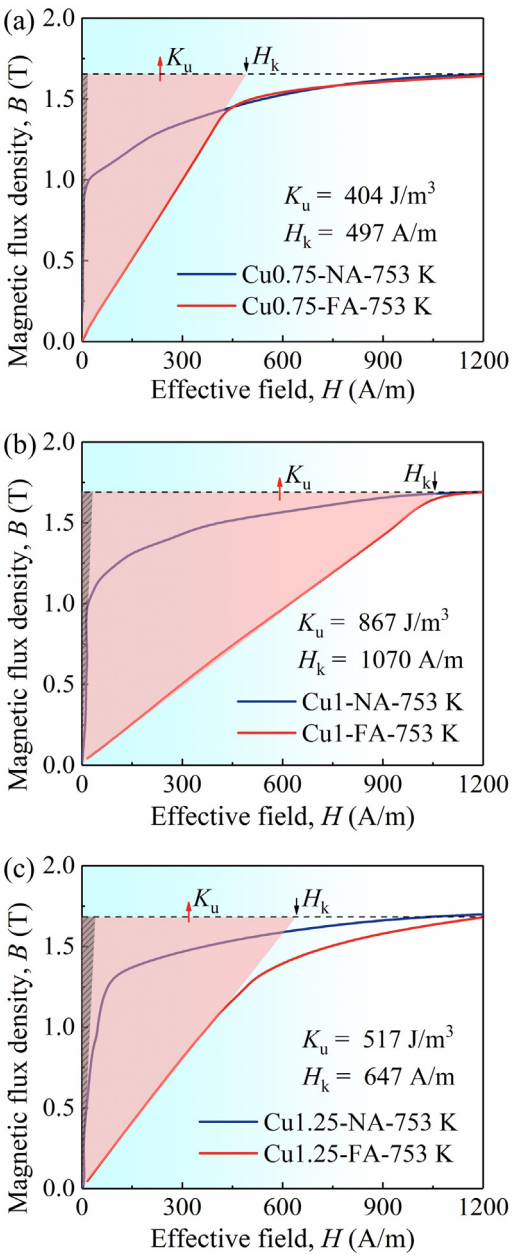

Fig. 6. Initial magnetization curves measured transversally and corrected for the demagnetization effect of (a) Cu0.75-NA/FA-753 K, (b) Cu1-NA/FA-753 K, (c) Cu1.25-NA/FA-753 K samples.

sition and nanostructure. The K_u is two orders of magnitude higher than the $\langle K_1 \rangle$, which reveals that the interplay between uniformly and locally induced magnetic anisotropies is the key factor affecting the soft-magnetic properties of these FA-treated nanocrystalline alloys. With an increase in K_u, the angular dispersion of the easiest axis decreases. Thus, compared to the Cu0.75-FA-753 K and Cu1.25-FA-753 K samples, the smaller local magnetic inhomogeneity in the Cu1-FA-753 K sample leads to its better soft-magnetic properties.

As the soft-magnetic properties and magnetic anisotropy are closely related to the magnetization process, the changes of magnetic domain recorded under static magnetic field are investigated for the Cu1-AQ, Cu1-NA-753 K, Cu1-FA-753 K, Cu0.75-FA-753 K and Cu1.25-FA-753 K samples as shown in Fig. 8. The Cu1-AQ sample exhibits wide-curved domain patterns of varying orientation, which reflects in-plane magnetic anisotropy resulting from

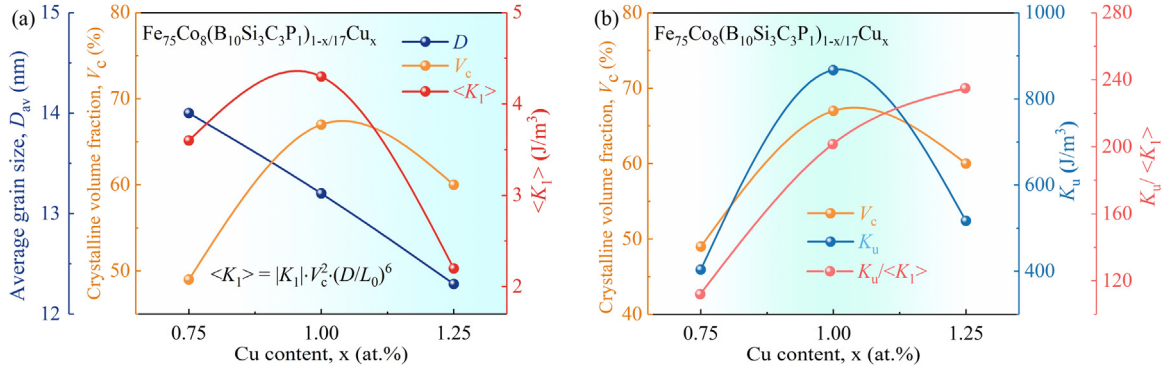

Fig. 7. (a) Variations of D_{av}, V_c and $\langle K_1 \rangle$ with the Cu content; (b) Variations of V_c, K_u and $K_u/\langle K_1 \rangle$ with the Cu content.

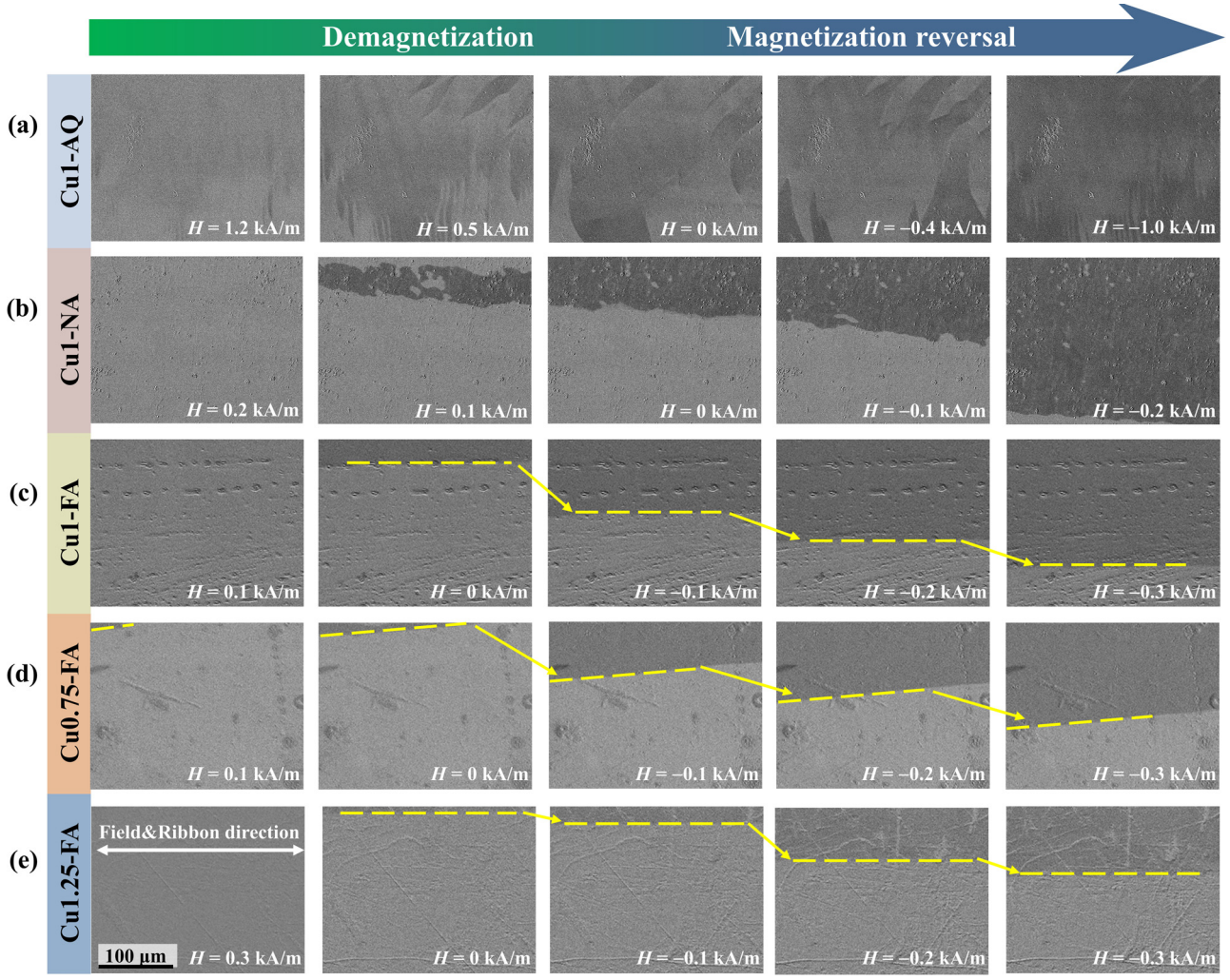

Fig. 8. Magnetization processes recorded under a static magnetic field for (a) Cu1-AQ, (b) Cu1-NA-753 K, (c) Cu1-FA-753 K, (d) Cu0.75-FA-753 K, and (e) Cu1.25-FA-753 K samples.

the magnetoelastic coupling of anisotropic internal stress field [43]. The processes of demagnetization and magnetization reversal are controlled by wall displacements, domain splitting and inhomogeneous rotations. The internal stress fluctuation with the wavelength comparable to domain wall width greatly pins the domain walls and is responsible for the poor soft-magnetic properties [44]. For the Cu1-NA-753 K sample, it can be seen that wide strip-like domains have irregular edges and patchy domains fluctuate on the micrometer scale within the wide domains. During the processes of demagnetization and magnetization reversal, these patchy domains act as nucleation sites and grow, and adjacent patchy domains merge to form larger domains, accompanied by the domain wall displacement. The patchy magnetization fluctuations are usually observed in nanocrystalline alloys and may be attributed to the random magneto-crystalline anisotropy for the Cu1-NA-753 K sample, which reveals a large angular dispersion of the easiest axis

from one region of exchange coupled grains to the other [45,46]. In addition, the incoherent magnetic anisotropy induced by the local spontaneous magnetization during NA treatment also contributes to the inhomogeneous magnetization processes and deteriorates the soft-magnetic properties [12]. For the Cu0.75/1/1.25-FA-753 K samples, regular wide domains with smooth edges are formed and the patchy domains disappear, which indicates that a homogeneous field-induced magnetic anisotropy dominates over the locally induced anisotropies and $\langle K_1 \rangle$ and decreases the angular dispersion of the easiest axes [47]. The processes of demagnetization and magnetization reversal occur by rapid wall displacement, explaining the significant improvement in magnetic softness. It can also be found that the domain walls gradually align longitudinally with the increase of K_u. Furthermore, the wall displacements of the Cu0.75-FA-753 K, Cu1-FA-753 K and Cu1.25-FA-753 K samples show distinct differences. With the increases of the magnetic field from 0 kA/m to 0.3 kA/m in the negative direction, domain walls have differences in the moving distance, with values of 119, 140 and 81 μm, respectively. The highest moving rate of the Cu1-FA-753 K sample results in its best soft-magnetic properties.

4. Conclusion

The $Fe_{75}Co_8(B_{10}Si_3C_3P_1)_{1-x/17}Cu_x$ (x = 0.75, 1, 1.25) nanocrystalline alloys with high B_s up to 1.87 T, high μ_e up to 16,000, low H_c of 1.6–3.0 A/m, and $P_{10/50}$ as low as 0.11 W/kg were obtained by FA method. The FA method increases the N_d and V_c, and refines the grains, leading to a decreased $\langle K_1 \rangle$ in comparison with the NA method. It is found that the application of a magnetic field during annealing promotes the nucleation and inhibits the diffusion of P atoms, which suppresses the grain growth and enhances the formation of (110) texture in the α-(Fe, Co) phase. In addition, the FA method induces longitudinal K_u two orders of magnitude higher than $\langle K_1 \rangle$, which is responsible for the formation of wide regular domains oriented longitudinally, the magnetization process dominated by pinning-free domain wall displacement, and thus the enhanced magnetic softness. The K_u reveals a dependence on the V_c, which rationalizes the differences in soft-magnetic properties and wall displacements for the FA samples with different Cu contents.

Data availability

The data that support the findings of this study are available from the corresponding author upon reasonable request.

Declaration of competing interest

The authors declare that they have no known competing financial interests or personal relationships that could have appeared to influence the work reported in this paper.

CRediT authorship contribution statement

Mingjuan Cai: Data curation, Formal analysis, Investigation, Methodology, Writing – original draft. **Zhijun Guo:** Funding acquisition, Methodology, Writing – review & editing. **Lei Li:** Data curation, Formal analysis, Investigation. **Xingyu Zheng:** Data curation, Formal analysis. **Xiaoxuan Yang:** Formal analysis, Investigation. **Qianqian Liu:** Formal analysis, Investigation. **Gaopeng Zou:** Formal analysis. **Baolong Shen:** Funding acquisition, Project administration, Supervision, Writing – review & editing.

Acknowledgments

This work was financially supported by the National Key R&D Program of China (No. 2022YFB3804100), the National Natural Science Foundation of China (No. 52231005), the Jiangsu Provincial Key R&D Program (No. BE2021088), and the Start-up Research Fund of Southeast University (No. RF1028623113).

References

[1] J.M. Silveyra, E. Ferrara, D.L. Huber, T.C. Monson, Science 362 (2018) eaao0195.
[2] D. Azuma, N. Ito, M. Ohta, J. Magn. Magn. Mater. 501 (2020) 166373.
[3] V.S. Tsepelev, Y.N. Starodubtsev, Nanomaterials 11 (2021) 108.
[4] X.S. Li, J. Zhou, L.Q. Shen, B.A. Sun, H.Y. Bai, W.H. Wang, Adv. Mater. (2022) 2205863.
[5] K. Suzuki, R. Parsons, B. Zang, K. Onodera, H. Kishimoto, A. Kato, Appl. Phys. Lett. 110 (2017) 012407.
[6] X.D. Fan, T. Zhang, W.M. Yang, J.H. Luan, Z.B. Jiao, H. Li, J. Mater. Sci. Technol. 147 (2023) 124–131.
[7] E. Lopatina, I. Soldatov, V. Budinsky, M. Marsilius, L. Schultz, G. Herzer, R. Schäfer, Acta Mater. 96 (2015) 10–17.
[8] L. Hou, X.D. Fan, Q.Q. Wang, W.M. Yang, B.L. Shen, J. Mater. Sci. Technol. 35 (2019) 1655–1661.
[9] M.J. Cai, J.J. Wang, Q.Q. Wang, Z.J. Guo, Q. Luo, J. Zhou, T. Liang, X.S. Li, Q.S. Zeng, B.L. Shen, Mater. Res. Lett. 11 (2023) 595–603.
[10] K. Hono, D.H. Ping, M. Ohnuma, H. Onodera, Acta Mater. 47 (1999) 997–1006.
[11] W. Betteridge, Prog. Mater. Sci. 24 (1980) 51–142.
[12] K. Suzuki, G. Herzer, Scr. Mater. 67 (2012) 548–553.
[13] G. Herzer, V. Budinsky, C. Polak, Phys. Status Solidi B 248 (2011) 2382–2388.
[14] L.K. Varga, Z. Gercsi, G. Kovács, A. Kákay, F. Mazaleyrat, J. Magn. Magn. Mater. 254-255 (2003) 477–479.
[15] X.J. Jia, W. Zhang, Y.Q. Dong, J.W. Li, A.N. He, J.H. Luan, R.W. Li, J. Alloy. Compd. 920 (2022) 166030.
[16] H. Fujii, V.A. Yardley, T. Matsuzaki, S. Tsurekawa, J. Mater. Sci. 43 (2008) 3837–3847.
[17] H. Fujii, S. Tsurekawa, T. Matsuzaki, T. Watanabe, Philos. Mag. Lett. 86 (2006) 113–122.
[18] M. Ohta, Y. Yoshizawa, Appl. Phys. Lett. 91 (2007) 062517.
[19] M. Ohta, Y. Yoshizawa, Appl. Phys. Express 2 (2009) 023005.
[20] M. Ohta, R. Hasegawa, IEEE Trans. Magn. 53 (2017) 2000205.
[21] K. Takenaka, M. Nishijima, A. Makino, IEEE Trans. Magn. 50 (2014) 2004704.
[22] L. Xie, A.D. Wang, S.Q. Yue, A.N. He, C.T. Chang, Q. Li, X.M. Wang, C.T. Liu, J. Magn. Magn. Mater. 483 (2019) 158–163.
[23] Z. Li, R. Parsons, H. Kishimoto, T. Shoji, A. Kato, J. Karel, K. Suzuki, J. Alloy. Compd. 902 (2022) 162544.
[24] X.D. Fan, H. Men, A.B. Ma, B.L. Shen, J. Magn. Magn. Mater. 326 (2013) 22–27.
[25] X.D. Fan, B.L. Shen, J. Magn. Magn. Mater. 385 (2015) 277–281.
[26] T. Liu, F.Y. Kong, L. Xie, A.D. Wang, C.T. Chang, X.M. Wang, C.T. Liu, J. Magn. Magn. Mater. 441 (2017) 174–179.
[27] R. Parsons, B. Zang, K. Onodera, H. Kishimoto, T. Shoji, A. Kato, K. Suzuki, J. Magn. Magn. Mater. 476 (2019) 142–148.
[28] K. Takenaka, A.D. Setyawan, P. Sharma, N. Nishiyama, A. Makino, J. Magn. Magn. Mater. 401 (2016) 479–483.
[29] J.H. Zhang, F.P. Wan, Y.C. Li, J.C. Zheng, A.D. Wang, J.C. Song, M.Q. Tian, A.N. He, C.T. Chang, J. Magn. Magn. Mater. 438 (2017) 126–131.
[30] L. Hawelek, T. Warski, P. Wlodarczyk, M. Polak, P. Zackiewicz, W. Maziarz, A. Wojcik, M. Steczkowska-Kempka, A. Kolano-Burian, Materials 14 (2021) 5.
[31] T. Warski, A. Radon, P. Zackiewicz, P. Wlodarczyk, M. Polak, A. Wojcik, W. Maziarz, A. Kolano-Burian, L. Hawelek, Materials 14 (2021) 726.
[32] Y.L. Jin, X.D. Fan, H. Men, X.C. Liu, B.L. Shen, Sci. China Technol. Sci. 55 (2012) 3419–3424.
[33] G. Herzer, Acta Mater. 61 (2013) 718–734.
[34] G. Herzer, J. Magn. Magn. Mater. 294 (2005) 99–106.
[35] G. Herzer, Scr. Metall. Mater. 33 (1995) 1741–1756.
[36] W.V. Youdelis, D.R. Colton, J. Cahoon, Can. J. Phys. 42 (1964) 2217–2237.
[37] S. Nakamichi, S. Tsurekawa, Y. Morizono, T. Watanabe, M. Nishida, A. Chiba, J. Mater. Sci. 40 (2005) 3191–3198.
[38] X.D. Wang, M. Qi, S. Yi, Scr. Mater. 51 (2004) 1047–1050.
[39] K. Hono, A. Inoue, T. Sakurai, Appl. Phys. Lett. 58 (1991) 2180–2182.
[40] L. Hu, R.R. Zhang, Q.W. Chen, Nanoscale 6 (2014) 14064–14105.
[41] P. Sharma, X. Zhang, Y. Zhang, A. Makino, Scr. Mater. 95 (2015) 3–6.
[42] N. Ito, K. Suzuki, J.S. Garitaonandia, J.D. Cashion, J. Appl. Phys. 105 (2009) 07A321.
[43] J.D. Livingston, W.G. Morris, J. Appl. Phys. 57 (1985) 3555–3559.
[44] H. Fujimori, Y. Obi, T. Masumoto, H. Saito, Mater. Sci. Eng. 23 (1976) 281–284.
[45] S. Flohrer, R. Schäfer, C. Polak, G. Herzer, Acta Mater. 53 (2005) 2937–2942.
[46] S. Flohrer, R. Schäfer, J. McCord, S. Roth, L. Schultz, G. Herzer, Acta Mater. 54 (2006) 3253–3259.
[47] S. Flohrer, G. Herzer, J. Magn. Magn. Mater. 322 (2010) 1511–1514.